Measurement of the anomalous spin precession frequency ω_a in the Muon $g-2$ experiment at Fermilab

Lorenzo Cotrozzi[a,b][*] **and Matteo Sorbara**[c] **for the Muon $g-2$ collaboration**

[a]*Università di Pisa (UniPi), Department of Physics "E. Fermi",*
Largo Bruno Pontecorvo 3/Building B, 56127 Pisa, Italy

[b]*INFN (Istituto Nazionale di Fisica Nucleare) - Pisa Section*
Largo Bruno Pontecorvo 3/Building C, 56127 Pisa, Italy

[c]*INFN (Istituto Nazionale di Fisica Nucleare) - Roma Tor Vergata Section*
Via della Ricerca Scientifica, 00133 Roma, Italy

E-mail: l.cotrozzi@studenti.unipi.it, matteo.sorbara@roma2.infn.it

The muon anomaly, $a_\mu = (g_\mu - 2)/2$, is a low-energy observable which can be both measured and computed to high precision, making it a sensitive test of the Standard Model (SM) and a probe for new physics. The current discrepancy between the experimental value and the Standard Model calculation from the Muon $g-2$ Theory Initiative is $a_\mu^{exp} - a_\mu^{SM} = (251 \pm 59) \cdot 10^{-11}$, with a significance of $4.2\,\sigma$. The Fermilab E989 experiment aims, with the full statistical power, to improve by a factor of four the precision of the measurement. In April 2021 the collaboration published the first measurement, based on the first year of data taking. This paper will present the status of the measurement of the anomalous muon spin precession frequency, ω_a, performed on the datasets collected during Run-2 and Run-3 (2019 and 2020 campaigns), with a preliminary projection of the systematic uncertainties.

[*]Speaker

1. The magnetic moment of the muon

The intrinsic magnetic moment of a charged particle with spin is defined by the following relation:

$$\vec{\mu} = g\frac{e}{2m}\vec{S}, \tag{1}$$

where e is the particle charge, m its mass, $\vec{S}$ its spin vector and g the so-called *g-factor* or *Landè factor*, a dimensionless parameter. The magnetic moment $\vec{\mu}$ gives us a measure of the torque $\vec{\tau} = \vec{\mu} \times \vec{B}$ and the energy $U = -\vec{\mu} \cdot \vec{B}$ that a charged particle experiences in a magnetic field. Dirac's equation predicts the value $g = 2$ for charged particles with $\frac{1}{2}$-spin such as electrons and muons, but deviations from 2, first measured by Kusch and Foley in 1948 [1], arise due to radiative corrections in the Standard Model (SM). We can define the magnetic anomaly of a lepton ℓ as:
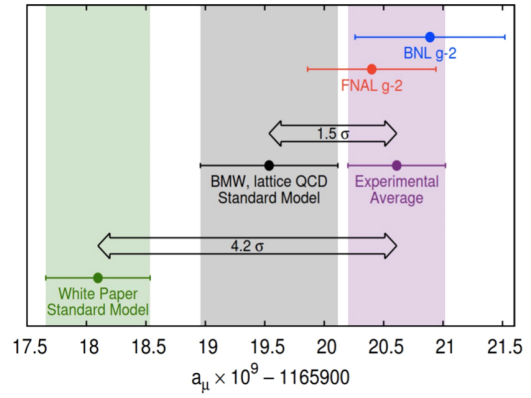
$$a_\ell = \frac{g_\ell - 2}{2} \qquad , \qquad \ell = e, \mu, \tau. \tag{2}$$

The anomaly can be decomposed into contributions from different interactions: $a_\mu = a_\mu^{\text{QED}} + a_\mu^{\text{Weak}} + a_\mu^{\text{QCD}}$. The dominant one is the 1-loop quantum electrodynamics (QED) correction to a_μ, computed by Schwinger in 1948 [2]: $a_e = \frac{\alpha}{2\pi} \simeq 0.00116$, where α is the fine structure constant. Schwinger's prediction was in agreement with Kusch and Foley's results. The quantum chromodynamics (QCD) contribution to a_μ amounts to ~ 60 parts per million (ppm) and carries the largest uncertainty on the muon magnetic anomaly. The leading term comes from Hadron Vacuum Polarization (HVP) diagrams, where the energy scale is of order of the muon mass, well below the region where QCD can be studied perturbatively: a dispersion relation approach is used to evaluate the contribution, using the total experimental cross section $\sigma_{tot}(e^+ e^- \rightarrow hadrons)$ [3]. Lattice QCD can

Figure 1: The Standard Model value recommended by the Muon $g-2$ Theory Initiative (green band) [6] is compared to the experimental average [5] and to the evaluation by BMW collaboration using lattice QCD (grey band) [4].

also be used to determine the HVP contribution to a_μ using an ab-initio calculation. In 2021, the BMW collaboration presented a prediction of a_μ^{HVP} which was in tension with the prediction from the dispersion approach [4]. Figure 1 presents the tension between the experimental average [5] and the value recommended by the $g-2$ Theory Initiative [6], which amounts to $a_\mu^{exp} - a_\mu^{SM} = (251 \pm 59) \cdot 10^{-11}$, and the tension between the two methods (dispersion approach and Lattice QCD) for predicting the hadronic contribution to a_μ.

2. Measurement principle of the $g-2$ experiment at Fermilab

When a charged particle with spin is placed in an uniform external magnetic field, it will follow a circular path because of the Lorentz force, with cyclotron frequency ω_C. Its spin will also precess around the direction of the magnetic field, with frequency ω_S. We define the anomalous precession frequency ω_a as follows:

$$\vec{\omega}_a = \vec{\omega}_S - \vec{\omega}_C = -\frac{e}{m}\left[a_\mu \vec{B} - a_\mu\left(\frac{\gamma}{\gamma+1}\right)\left(\vec{\beta} \cdot \vec{B}\right)\vec{\beta} - \left(a_\mu - \frac{1}{\gamma^2-1}\right)\frac{\vec{\beta} \times \vec{E}}{c}\right]. \tag{3}$$

In the $g-2$ experiment, muons are stored in a 1.45 T magnetic field and electrostatic quadrupole (ESQ) plates provide weak focusing for vertical confinement. Ideally, the second term in Eq. (3) vanishes for muons that travel orthogonally to the magnetic field, $\vec{\beta} \cdot \vec{B} = 0$, and the third term vanishes for muons with the "magic momentum" $p_\mu \simeq 3.09$ GeV/c, so that $\gamma = \sqrt{1 + \frac{1}{a_\mu}} \simeq 29.3$. Corrections introduced by these terms are described in Ref. [7]. In this configuration, the expression for the anomalous precession frequency becomes $\omega_a = a_\mu \left(\frac{e}{m} \right) B \simeq 1.43$ rad/µs, whereas the cyclotron frequency is $\omega_C \simeq 42$ rad/µs.

The magnetic field can be expressed by means of the Larmor precession frequency of free protons, via $\hbar \omega_p = 2\mu_p |\vec{B}|$, so that $a_\mu = \frac{\omega_a}{\omega_p} \frac{\mu_p}{\mu_e} \frac{m_\mu}{m_e} \frac{g_e}{2}$. In this paper we will focus on the measurement of ω_a, which can be fitted from the time distribution of decay positrons detected by calorimeters. The determination of ω_p is described in Ref. [8].
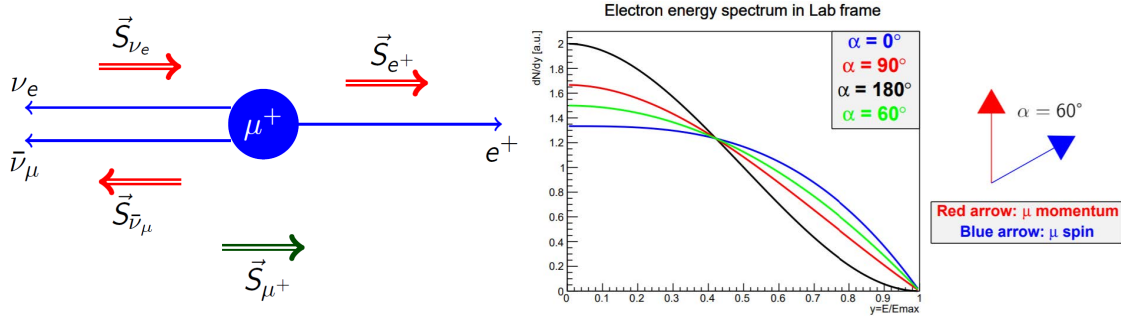
Figure 2: *Left*: Diagram of muon decay in the center-of-mass frame. *Right*: Energy spectrum of emitted positron in $g-2$ laboratory frame, which changes as a function of the anomalous precession phase.

Due to parity violation in the muon weak decay, high energy positrons are emitted preferentially in the muon's spin direction in the center-of-mass frame (Figure 2, *left*). As a consequence, in the lab frame the energy spectrum of emitted positrons has a different shape depending on the angle between muon spin and muon momentum, i.e. the anomalous precession phase (Figure 2, *right*). If we take the integral of the spectrum above a fixed threshold, which corresponds to counting all positrons above a certain energy, we will find a distribution that is modulated by the ω_a frequency, described - in the ideal case - by Eq. (4):

$$N(t) = N_0 e^{-t/\gamma\tau} \left[1 + A_0 \cos\left(\omega_a t + \phi_a \right) \right], \tag{4}$$

where $\gamma\tau$ is the muon lifetime in the lab frame, ~ 64.4 µs. The optimal threshold that minimizes the statistical uncertainty on ω_a is 1.7 GeV [9].

3. Positron detection and reconstruction

Positrons that are emitted from muon decay have a smaller orbit radius than the muon beam, thus they curl towards the center of the ring where they are detected (Figure 3, *right*). There are 24 electromagnetic calorimeters placed around the inner radius of the storage ring, which measure the energies and arrival times of incident positrons. Each segmented calorimeter features a 6×9 matrix of PbF_2 (lead fluoride) crystals, with size $2.5 \times 2.5 \times 14$ cm^3, transparent to visible light. Each crystal absorbs the energy of incoming positrons by generating an electromagnetic shower, which is contained thanks to $\sim 15 X_0$ of crystal length and a Molière radius of 1.8 cm. The generated charged

particles travel faster than light in the crystal (refractive index $n \simeq 1.8$), so they generate Cherenkov photons. Each crystal is coupled to a silicon photomultiplier (SiPM), shown in Figure 3 (*left*), which responds to Cherenkov photons with electrical current; this current is then converted into voltage signal by a custom electronic board, recorded by waveform digitizers and stored for offline analysis. A laser calibration system sends simultaneous pulses onto each of the 1296 crystals, to monitor the SiPM gains at the level of 0.04% during the 700 μs window in which muons are stored, and also on the timescales of days and months to correct for long-term effects, such as temperature changes [10].
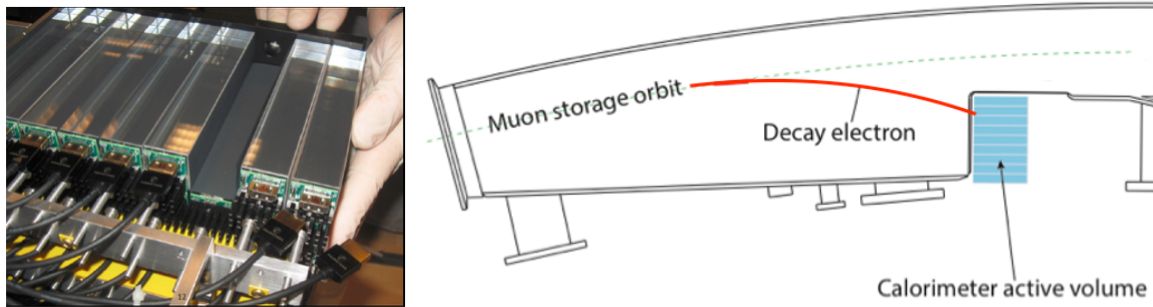
Figure 3: *Left*: Picture of PbF$_2$ crystals during calorimeter assembly, each coupled to a SiPM board (green). *Right*: Trajectory of emitted electron from muon decay, detected by the calorimeter.
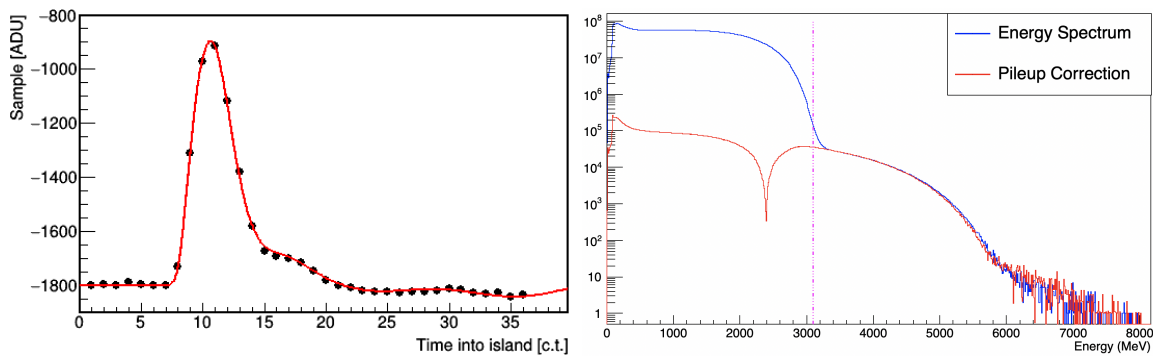

Figure 4: *Left*: Trace of a positron hitting a crystal, fitted with a predetermined template to obtain the time and deposited energy of the event. *Right*: Energy spectrum of clusters before pileup correction (blue) and absolute value of the correction (red), which would be positive until ∼ 2.38 GeV and negative after that value.

To reconstruct the energy and arrival time of detected positrons, we perform a template fit on the waveforms of each crystal hit, as shown in the example in Figure 4 (*left*). We then reassemble all of the crystal hits to reconstruct the events and fill a two-dimensional histograms, in energy and time. When two or more positrons hit the same calorimeter very close in time, the reconstruction algorithm is not always able to separate the two events and the incident particles are reconstructed as a single hit. This is the pileup effect and it introduces a systematic bias in the ω_a analysis because it distorts the measured energy and time spectra in a time-dependent way: the rate of double-events is the square of the rate of detected positrons, so it has a lifetime of ∼ 32 μs. By studying the time distribution of clusters, we estimate the number of double and triple pileup events that need

to be subtracted, as well as the number of single events that need to be added: we apply the pileup correction to all energy and time bins in our histograms. Figure 4 (*right*) shows the energy spectrum of positrons before pileup subtraction, where values above the maximum physical energy of 3.1 GeV are present, and the absolute value of the applied correction, which reduces the component above 3.1 GeV. The production workflow from stored raw data to positron events is described in Ref. [11].

4. Precession frequency analysis: fit to "wiggle plots"

From the pileup-corrected energy and time distribution of the positrons, there are different methods to build the histograms used to extract the anomalous precession frequency ω_a: this paper will focus on the "Threshold method" (T-Method) which was commonly used amongst most analysis groups. The time distribution of detected positrons above the 1.7 GeV threshold is shown in the upper plot of Figure 5 (*left*), and it is called "wiggle plot" due to its shape. In principle, we can perform a very simple fit with the 5 parameters of Equation (4): N_0, $\gamma\tau$, A_0, ω_a and ϕ_a. Figure 5 (*left*) shows the fit to data and the residuals: an oscillating term is present in the residuals, mostly due to beam dynamics effects which must be accounted for to avoid systematic biases to ω_a. If we take the Fast Fourier Transform (FFT) of the residuals we obtain the red dashed curve in Figure 5 (*right*) where the peaks are all of the frequencies that appear in the residuals.
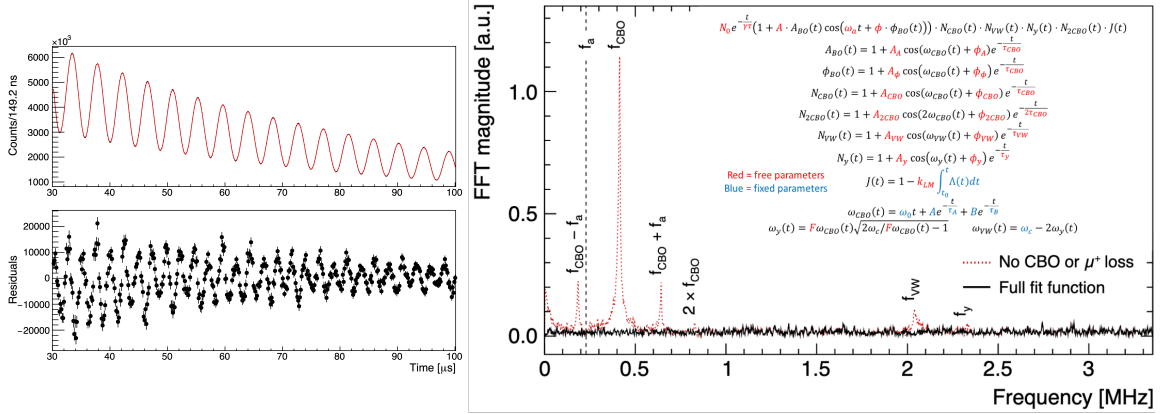
Figure 5: *Left*: 5-parameter fit to positron time distribution (*upper*) and fit residuals (*lower*). *Right*: FFT of residuals in the case of 5-paremeter function (dashed red) or complete fit function in Run-1 (solid black).

The dominant frequency is due to the "Coherent Betatron Oscillation" (CBO): the muon beam in the storage ring oscillates radially with frequency $\omega_x \simeq 40\,\mathrm{rad/\mu s}$, smaller than the cyclotron frequency, so the wavelength of the radial oscillation is greater than the ring circumference. Each of the 24 calorimeters samples the positron distribution at a fixed location, so the rate at which the muon bunch moves with respect to the detector is the CBO frequency: $\omega_{CBO} \equiv \omega_C - \omega_x \simeq 2.32\,\mathrm{rad/\mu s}$. The peak at very low frequencies, instead, is due to the "muon loss" term: muons during fill time can be scattered away from the storage ring, typically because they interact with collimators or because the injection angle differs from the design value, so they reduce the detected positrons in a time-dependent way. Figure 5 (*right*) shows the complete fit function with 22 free parameters that we used in Run-1 to fit data: the CBO terms are shown, as well as the $J(t)$ function that corrects for muon loss, and also other terms for vertical beam oscillations. The solid black curve is the FFT of residuals when fitting with the complete function, where all previous peaks have vanished.

5. Systematic studies and expected uncertainties for Run-2 and Run-3

There are many sources of systematic uncertainties to ω_a, most of them related to how well we know the parameters used in positron reconstruction, such as pileup subtraction or energy calibration, or to how well we understand the beam dynamics effects in our time distributions. In Run-1, the biggest systematic contributions to ω_a were pileup, which amounted to 35 parts per billion (ppb), and CBO that contributed for 38 ppb. The total uncertainty on ω_a was 434 ppb due to statistics and 56 ppb from systematic effects [12]. In Run-2 and Run-3, we collected 4.5 times more statistics than Run-1, so we expect a statistical uncertainty of $\simeq 200$ ppb; in addition, there were many hardware and software improvements to reduce the systematics. For instance, the non-ferric fast kicker system was fixed to provide a stronger kick to the muon beam and facilitate its centering; damaged resistors in the electrostatic quadrupole system, which strongly affected the beam dynamics introducing an additional systematic uncertainty of 75 ppb, were replaced. On the reconstruction side, we improved our algorithms to better resolve pileup. Thanks to these improvements, for Run-2 and Run-3 results we expect a significant reduction to ω_a systematics with respect to Run-1.

Acknowledgments

References

[1] P. Kusch and H. M. Foley, *The Magnetic Moment of the Electron*, *Phys. Rev.* **74**, 250 (1948).

[2] J. S. Schwinger, *On Quantum-Electrodynamics and the Magnetic Moment of the Electron*, *Phys. Rev.* **73**, 416 (1948).

[3] M. Davier *et al.*, *A new evaluation of the hadronic vacuum polarisation contributions to the muon anomalous magnetic moment and to $\alpha(m_Z^2)$*, *Eur. Phys. J. C* **80**, 241 (2020) [hep-ph/1908.00921].

[4] Sz. Borsanyi *et al.*, *Leading hadronic contribution to the muon magnetic moment from lattice QCD*, *Nature* **593**, 51-55 (2021) [hep-lat/2002.12347].

[5] B. Abi *et al.* (Muon $g-2$ Collaboration), *Measurement of the Positive Muon Anomalous Magnetic Moment to 0.46 ppm*, *Phys. Rev. Lett.* **126**, 141801 (2021) [hep-ex/2104.03281].

[6] T. Aoyama *et al.*, *The anomalous magnetic moment of the muon in the Standard Model*, *Phys. Rep.* **887**, 1 (2020) [hep-ph/2006.04822].

[7] A. Driutti (Muon $g-2$), PoS(ICHEP2022) , 053 (2022), these proceedings.

[8] R. Reimann (Muon $g-2$), PoS(ICHEP2022) , 054 (2022), these proceedings.

[9] G. W. Bennett *et al.*, *Statistical equations and methods applied to the precision muon $(g-2)$ experiment at BNL*, *Nucl. Instrum. Meth. A* **579**, 1096 (2007).

[10] A. Anastasi *et al.*, *The laser-based gain monitoring system of the calorimeters in the Muon $g-2$ experiment at Fermilab*, *JINST* **14**, P11025 (2019) [physics.ins-det/1906.08432].

[11] P. Girotti (Muon $g-2$), PoS(ICHEP2022) , 228 (2022), these proceedings.

[12] T. Albahri *et al.* (Muon $g-2$ Collaboration), *Measurement of the anomalous precession frequency of the muon in the Fermilab Muon $g-2$ experiment*, *Phys. Rev. D* **103**, 072002 (2021) [hep-ex/2104.03247].